

Wetter

STUDIES OF FUNDAMENTAL INTERACTIONS USING MOLECULES

E. A. Hinds

Physics Department, Yale University, New Haven, Connecticut 06520

**A series of Lectures Presented at
the 44th Scottish Universities Summer School in Physics
15-26 August 1994, Stirling, Scotland.**

STUDIES OF FUNDAMENTAL INTERACTIONS USING MOLECULES

Introduction

This course is about a series of experiments at Yale University using molecular beams to study fundamental questions in physics. The central topic is the search for information about time-reversal (T) symmetry in elementary particle interactions. The experimental approach is to observe the electric dipole interaction between a molecule and an external electric field and to search for a part of the energy that changes sign when the electric field is reversed. In this way it is possible, as we shall see, to learn about T symmetry in the nucleus, in the electrons and in the interaction between the two. In addition, we discuss the Aharonov-Casher geometric phase, which is also concerns the dipole interactions of a neutral particle with external fields, although in that case we are interested in normal (T-conserving) electromagnetic interactions.

In lecture 1, I provide some background information about the discrete symmetries C, P, and T and discuss how they are connected with the electric dipole moment (EDM) of an atomic system. This leads to a discussion of Schiff's theorem and of the mechanisms which allow an atom to have an EDM. In this lecture I focus on the finite nuclear size mechanism or volume effect, leaving relativistic effects for lecture 4.

Lecture 2 begins by making the distinction between nuclear-spin-dependent and electron-spin-dependent T-violation. This is followed by an account of our molecular beam experiment on TIF, which is an example of the former since it looks for T-violation associated with the Tl nuclear spin.

In lecture 3, I recall the main points about the Aharonov-Bohm and Aharonov-Casher phases and describe the various effects one might hope to see. There follows an account of our high-precision test of the Aharonov-Casher phase, which was done using the TIF molecular beam.

Returning to Schiff's theorem and relativistic effects, I show in Lecture 4 how the electron EDM can give rise to an atomic EDM. This leads to a discussion about the use paramagnetic molecules to determine the electron EDM and an evaluation of which are the most promising candidates. Finally, I describe the status of our own work on the YbF molecule and the prospects for using it to measure the electron EDM.

LECTURE 1

Discrete symmetries, Schiff's theorem, and the volume effect

A. Discrete Symmetries

There are three interrelated reflection symmetries to consider: space inversion (parity, P), interchange of particles and anti-particles (charge conjugation, C), and time reversal (T). Until the early 1950's, it was thought to be axiomatic that all of these were symmetry operation, i.e. that the properties of physical systems were invariant under the action of any of them. This point of view was challenged by Purcell and Ramsey (1950) who proposed looking for a permanent electric dipole moment (EDM) of the neutron, and by Lee and Yang (1956) who discussed in some detail the possibility that weak interactions may not have parity symmetry. In 1957 a famous experiment by Wu et al. (1957) showed that weak interactions do indeed violate P symmetry very strongly (in fact, maximally). The method they used was to polarize ^{60}Co nuclei in a cryostat by means of nuclear demagnetization and to search for a correlation $\langle \vec{\sigma} \cdot \vec{p} \rangle$ between the nuclear spin $\vec{\sigma}$ and the momentum \vec{p} of the electron emitted in β - decay. They found the strong correlation shown schematically on the left of Fig. 1.1, in which the electrons prefer the left-handed final state $\vec{\sigma} \cdot \vec{p} < 0$ to the right handed version $\vec{\sigma} \cdot \vec{p} > 0$. Since this property ($\vec{\sigma} \cdot \vec{p} < 0$) is not invariant under space inversion, P is violated somewhere in the system. The left-handedness of weak interaction is now a very well established phenomenon, tested by numerous experiments in particle, nuclear, and atomic physics (Commins and Bucksbaum 1983).

Soon after the discovery of P-violation, Landau (1957) proposed that symmetry might not be entirely lost; the combined action CP of charge conjugation and space inversion could still be a symmetry operation. To illustrate the point, I imagine (somewhat unrealistically) repeating the cobalt experiment with anti-cobalt. With CP symmetry the rates must be exactly equal and the angular distributions exactly opposite. In that case, the world under CP inversion is indistinguishable from the real world, as illustrated in Fig. 1.2; P-violation and C-violation conspire to produce CP symmetry.

This happy resolution of broken P-symmetry did not last long. In 1964 Christenson et al. discovered that the long-lived neutral kaon, K_L^0 , can decay occasionally into two pions as well as the more usual three. Since the 2π and 3π final states have opposite CP symmetry, one is forced to conclude that K_L^0 is not an eigenstate of CP and/or the decay process itself can change the CP symmetry of the system. In either case CP symmetry is violated. Our current understanding is that K_L^0 is close to being an equal antisymmetric superposition $\frac{1}{\sqrt{2}}(K^0 - \bar{K}^0)$ of the strong eigenstate K^0 and its charge conjugate \bar{K}^0 . If the two coefficients were exactly equal to $\pm 1/\sqrt{2}$, this state could not decay into 2π because the amplitudes for $K^0 \rightarrow 2\pi$ and $\bar{K}^0 \rightarrow 2\pi$ would cancel. The small decay branch ($\sim 2 \times 10^{-3}$) into 2π indicates that this cancellation is not perfect, and it is thought that indeed the K_L^0 spends a little more of its time being a K^0 than it does being a \bar{K}^0 . This CP non-symmetric state is illustrated in Fig. 1.3.

If nature is described by a relativistic local field theory, then symmetry is still not entirely lost because the even more complicated transformation CPT is necessarily a symmetry operation (the CPT theorem) (Paul 1955). In that case T symmetry must be violated in just the right way to make up for CP-violation. The role of T-violation can be seen in the following simple model. CPT invariance tells us that K^0 and \bar{K}^0 have the same mass, width and internal degrees of freedom. Nevertheless the dynamic equilibrium of $K^0 \leftrightarrow \bar{K}^0$ produces the unbalanced state in Fig. 1.3. This implies that the rate $K^0 \rightarrow \bar{K}^0$ is faster than the reverse process $\bar{K}^0 \rightarrow K^0$, in violation of T symmetry. In the rest of this course we will assume the validity of the CPT theorem and will refer to T violation and CP-violation interchangeably.

We come back now to the beginning of this section and the proposal by Purcell and Ramsey that the neutron may have an EDM. Fig. 1.4 shows that the existence of a neutron EDM would indicate a violation of P-symmetry since the EDM must reverse relative to the angular momentum $\vec{\sigma}$ under space inversion P. A similar argument, also illustrated in Fig. 1.4, shows that the EDM violates T-symmetry as well. When Smith et al. (1957) measured the neutron EDM, they obtained a result consistent with zero, and after 37 years, although the precision has been improved enormously, the result is still consistent with zero. Since we know that P-symmetry is violated by the weak interaction, this indicates a very high degree of T-symmetry in the neutron. This seems to be generally true. Apart from the kaon system, no instance of T-symmetry violation has been found anywhere despite a large number of searches in atomic, nuclear, and particle physics. In this course I will discuss new possibilities for detecting T-violation by molecular spectroscopy on a diatomic

molecule. The basic idea (as with the neutron and with atoms) is to look for an EDM due to some P- and T-violating interaction within the molecule. Whereas the normal dipole moment lies among the internuclear axis and vanishes on average (except in the co-rotating frame), this T-violating EDM is along the angular momentum and is nonzero, even in zero electric field.

B. Schiff's Theorem

Let us suppose that one of the particles making up our molecule (e.g., the electron or proton) has an intrinsic EDM. This should induce an EDM of the molecule, which could be detected by looking at the interaction with an external field \vec{E}_{ext} . Of course the field also induces a dipole moment, giving rise to the normal Stark shift, but the two can be distinguished simply by reversing the sign of \vec{E}_{ext} . This changes the sign of the T-violating interaction but not the usual Stark effect.

Let us approximate an atom or molecule as a nonrelativistic collection of point charges interacting only through Coulomb forces. To begin, we will take the EDMs of all the charged particles to be zero. In an external electric field \vec{E}_{ext} , the Hamiltonian can be written as a sum of kinetic and potential terms $H^0 = T + V$ where V includes the external potential. Now let particle i at position \vec{r}_i have a small EDM \vec{d}_i . This interacts with the total electric field $\vec{E}(\vec{r}_i)$ at \vec{r}_i according to

$$H^1 = -\vec{d}_i \cdot \vec{E}(\vec{r}_i) = \vec{d}_i \cdot [\vec{\nabla}_i, V/q_i] \quad (1.1)$$

The kinetic term T in our nonrelativistic Hamiltonian H^0 commutes with $\vec{\nabla}_i$, so we may equally well write

$$H^1 = \left[\frac{\vec{d}_i \cdot \vec{\nabla}_i}{q_i}, H^0 \right] \quad (1.2)$$

The first-order contribution of H^1 to the energy of the system is $\langle \psi^0 | H^1 | \psi^0 \rangle$, where $|\psi^0\rangle$, the unperturbed state, is an eigenfunction of H^0 . Because H^1 can be written as a commutator with H^0 (Eq. (1.2)), this diagonal matrix element vanishes. We conclude therefore that in an applied electric field \vec{E}_{ext} , there is no interaction energy to first order in \vec{d}_i ; the atom or molecule has no permanent EDM even if the constituents do!

This is generally called Schiff's theorem, although Schiff's famous paper (1963) is mainly devoted to showing how first-order effects *can* occur in spite of the theorem. Schiff proposed two mechanisms. (i) The volume effect: particles are not points, but extended objects with distributions ρ_c of charge and ρ_d of electric dipole moment. (ii) The relativistic effect: when the problem is treated relativistically, H^1 can no longer be written as a commutator with H^0 . In the rest of this lecture I will discuss the case of a nonrelativistic atom in which the nucleus has finite size and EDM, giving rise to a first-order energy shift in an external field through the volume effect.

C. Volume Effect

Let the nucleus have charge Q_N and an electric dipole moment \vec{D}_N . The expectation value of \vec{D}_N must lie along the nuclear angular momentum direction $\vec{\sigma}$, allowing us to define $\langle \vec{D}_N \rangle = D_N \vec{\sigma}$. Let the charge in an elementary volume d^3x of the nucleus be $Q_N \rho_c(\vec{x}) d^3x$ and let the EDM of the element be $D_N \vec{\sigma} \rho_d(\vec{x}) d^3x$. (We are assuming for the sake of simplicity that the spin of each volume element averages along the axis of total spin.) This defines the distributions ρ_c and ρ_d of charge and EDM. For a neutral atom or molecule, there is no average force on the nucleus, even in the presence of an uniform applied electric field \vec{E}_{ext} , so

$$\langle \vec{F}_N \rangle = Q_N \int d^3x \rho_c \langle \psi^0 | \vec{E}(\vec{x}) | \psi^0 \rangle = 0. \quad (1.3)$$

Here $\vec{E}(\vec{x})$ is the total electric field at the nuclear volume element d^3x due to both \vec{E}_{ext} and the electrons. The electric dipole interaction energy is

$$\langle H^1 \rangle = -D_N \vec{\sigma} \cdot \int d^3x \rho_d \langle \psi^0 | \vec{E}(\vec{x}) | \psi^0 \rangle. \quad (1.4)$$

Since $\langle \vec{F}_N \rangle = 0$, we are free to add $\vec{\sigma} \cdot \langle \vec{F}_N \rangle D_N / Q_N$ to Eq. (4), with the result

$$\langle H^1 \rangle = -D_N \vec{\sigma} \cdot \int d^3x (\rho_d - \rho_c) \langle \psi^0 | \vec{E}(\vec{x}) | \psi^0 \rangle. \quad (1.5)$$

When $\rho_d = \rho_c$, as in the case of a point nucleus, we recover Schiff's theorem ($\langle H^1 \rangle = 0$). Since it follows from the vanishing of $\langle \vec{F}_N \rangle$, we see that Schiff's theorem is related to the shielding of the

external field by the electrons. In fact each particle is shielded from \vec{E}_{ext} by the polarization of the others. However, if ρ_d differs from ρ_c , \vec{E}_{ext} is not entirely hidden from the EDM and the residual interaction is given by Eq. (1.5).

a) The field $\vec{E}(\vec{x})$

We turn now to the evaluation of Eq. (1.5), which requires an explicit form for $\vec{E}(\vec{x})$:

$$\vec{E}(\vec{x}) = \vec{E}_{\text{ext}} - \frac{e}{4\pi\epsilon_0} \sum_i \vec{\nabla}_{\vec{r}_i} \frac{1}{|\vec{x} - \vec{r}_i|} \quad (1.6)$$

In order to keep the notation as simple as possible, I will use cgs atomic units here (set $e/4\pi\epsilon_0 = 1$) and drop the explicit summation over electrons. Now we make a multipole expansion of $|\vec{x} - \vec{r}|^{-1}$, keeping only the monopole term in \vec{x} .

$$\begin{aligned} \vec{E}(\vec{x}) &= \vec{E}_{\text{ext}} + \frac{\hat{r}}{r^2} \theta(r - x) + \text{higher multipoles in } \vec{x} \\ &= \vec{E}_{\text{ext}} + \frac{\hat{r}}{r^2} [1 - \theta(x - r)] + \text{higher multipoles in } \vec{x}, \end{aligned} \quad (1.7)$$

where θ is the Heaviside step function.

In this lecture, we consider only the case of a spherical nucleus. With spherical ρ_c and ρ_d the higher multipoles of Eq. (1.7) contribute nothing to the integral over d^3x in Eq. (1.5) and they can be omitted. Also the first two terms of Eq. (1.7) contribute nothing because \vec{E}_{ext} and \hat{r}/r^2 are independent of \vec{x} and $\int d^3x (\rho_d - \rho_c) = 0$. Thus we can make the effective replacement

$$\vec{E}(\vec{x}) \Rightarrow \frac{\hat{r}}{r^2} \theta(x - r) \quad (1.8)$$

which acts only on electron *inside* the nucleus, and yields

$$\langle \psi^0 | \vec{E}(\vec{x}) | \psi^0 \rangle \Rightarrow - \int_0^x r^2 dr \int_0^{4\pi} d\Omega \psi^{0*} \frac{\hat{r}}{r^2} \psi^0 \quad (1.9)$$

Since \hat{r} is an odd parity operator, this must vanish unless ψ^0 is a state of mixed parity, as it is when in the external field \vec{E}_{ext} . In non-zero external field, we can expand ψ^0 in hydrogenic partial waves around the nucleus

$$\psi^0(r) = a_s Z^{1/2} Y_0^0 + a_p Z^{3/2} r Y_0^1 + \dots \quad (1.10)$$

where the first two terms are the S and P waves and terms of higher angular momentum l involve factors r^l . We have factored out explicitly the dependence on nuclear charge Z from the amplitudes a_s and a_p . Since the nuclear radius is $\sim 10^{-4}$ (we are still using atomic units), the contributions of higher partial waves to $\langle \vec{E}(\vec{x}) \rangle$ are strongly suppressed and we will assume they are negligible in comparison with the s-p contribution. Then

$$\langle \psi^0 | \vec{E}(\vec{x}) | \psi^0 \rangle \Rightarrow -x^2 Z^2 \frac{a_s a_p}{\sqrt{3}} \hat{\lambda}, \quad (1.11)$$

where $\hat{\lambda}$ is the axis of the electronic s-p mixing. Now that we have an effective expression for the field, we can return to the main theme; evaluation of Eq. (1.5), the volume effect.

b) The Schiff Moment

Inserting Eq. (1.11) into Eq. (1.5) we obtain $\langle H^1 \rangle$ as a product of a nuclear factor and an electronic factor.

$$\langle H^1 \rangle = \left[\frac{1}{6} D_N \int d^3x (\rho_d - \rho_c) x^2 \vec{\sigma} \right] \cdot \left[6Z^2 \frac{a_s a_p}{\sqrt{3}} \hat{\lambda} \right] \quad (1.12)$$

The nuclear part is known as the Schiff moment $Q\vec{\sigma}$

$$Q = \frac{1}{6} D_N \int d^3x (\rho_d - \rho_c) x^2 \quad (1.13)$$

c) The Schiff Interaction

Consider the derivative $[\vec{\nabla} \nabla^2 V]_0$ of the potential due to the electron evaluated

at the origin. This is related to the electron density through Poisson's equation. Still in cgs atomic units,

$$\vec{\nabla} \nabla^2 V = -4\pi \vec{\nabla} \rho = 4\pi \vec{\nabla} |\psi^0|^2 \quad (1.14)$$

using Eq. (1.10) we obtain

$$[\vec{\nabla}\nabla^2V]_0 = 6Z^2 \frac{a_s a_p}{\sqrt{3}} \hat{\lambda}. \quad (1.15)$$

Collecting together Eqs. (1.12), (1.13), (1.15) we find

$$\langle H^1 \rangle = Q \vec{\sigma} \cdot [\vec{\nabla}\nabla^2V]_0 \quad (1.16)$$

This interaction is what remains as a result of the finite nuclear size when the electric dipole interaction is suppressed by Schiff's theorem. We call it the Schiff interaction.

An Aside

One can recognize the Schiff interaction as the first non-zero term in a Taylor expansion. Loosely speaking we expand $\langle \psi^0 | \vec{E}(\vec{x}) | \psi^0 \rangle$ in Eq. (1.5) around the center of charge as

$$\langle \vec{E}(\vec{x}) \rangle \sim E(0) + xE' + x^2E'' + \dots \quad (1.17)$$

in which $E(0) = 0$ because the force must be zero. The first-derivative term xE' contributes nothing to the integral over the nucleus (Eq. (1.5)) because it has odd parity. Hence the leading effect is due to x^2E'' which yields in Eq. (1.5)

$$\langle H^1 \rangle = -D \vec{\sigma} \cdot \langle (\rho_d - \rho_c) x^2 E'' \rangle \quad (1.18)$$

Since $E'' \sim -V'''$, this has all the essential features of the more rigorous Eq. (1.16).

The Schiff Moment is Actually More General

In deriving the Schiff moment Q (Eq. (1.13)), we assumed a spherical distribution $\rho_a \vec{\sigma}$ of electric dipole moment due, for example, to an intrinsic EDM of the proton or neutron. But even when the nucleons have no EDM, it is still possible for the nucleus to acquire a dipole distortion if the forces between nucleons violate P and T symmetry. If the dipolar part of the charge distribution is $\delta(\vec{x})$, we can define the distributed EDM as $\vec{d} = \vec{x} \delta(\vec{x})$, and the total EDM as $D_N \vec{\sigma} = \int d^3x \vec{d}$. It can be shown (from the V''' term in a Taylor expansion of $V(\vec{x})$) (Sushkov et al. 1984) that once again there is a Schiff interaction of the form given in Eq. (1.16), with the Schiff moment being given now by

$$Q = \frac{1}{6} \int d^3x \left[\frac{3}{5} \vec{d} - D_N \rho_c \vec{\sigma} \right] x^2 \quad (1.19)$$

d) Conclusions about the Volume Effect

The volume effect leads to an effective interaction given by Eq. (1.16) which is the product of two parts. The first is the Schiff moment $Q\vec{\sigma}$ and it is of order $D_N r_N^2$ where r_N is the nuclear radius (see Eqs. (1.13), (1.19)). Q is sensitive to the EDM of the nucleons (due, for example, to P & T-odd interactions between the quarks) and to a dipole distortion of the nuclear charge (due for example to P & T-odd interactions between nucleons). The second part is the electronic factor $[\vec{\nabla}^2 V]_0$, which is proportional to the gradient of electron density at the nucleus. This can be related to the $l=0$ and $l=1$ parts of the electronic wavefunction by Eq. (1.15). In systems where neither the s nor the p part of the wavefunction is large, the Schiff interaction is suppressed since higher partial waves have a factor $(r_N/a_0)^l$ at the origin.

Schiff Interaction in an Atom

For an atom in an s state, the polarization induced by the electric field \vec{E}_{ext} is due to an s-p admixture given to first order in \vec{E}_{ext} by

$$a_s a_p \hat{\lambda} = \sum_n \frac{\langle s | e z | np \rangle}{W_{np} - W_s} \vec{E}_{\text{ext}} \quad (1.20)$$

For a very rough numerical estimate, we take $\langle s | e z | np \rangle \sim 1 \text{ au}$, and $W_{np} - W_s \sim 1 \text{ au}$, and hence $a_s a_p \hat{\lambda} \sim \vec{E}_{\text{ext}}$ in atomic units (1 a.u. of electric field is $5 \times 10^9 \text{ V/cm}$). Equation (1.15) then gives $[\vec{\nabla}^2 V]_0 \sim 4Z^2 \vec{E}_{\text{ext}}$. With $Q \sim D_N r_N^2$ it follows from Eq. (1.16) that the Schiff interaction is

$$\langle H^1 \rangle \sim D_N \vec{\sigma} \cdot 4Z^2 (r_N/a_0)^2 \vec{E}_{\text{ext}}, \quad (1.21)$$

where we have written the Bohr radius explicitly in order to return to normal units. Since $r_N/a_0 \sim 10^{-4}$, we find that in a heavy atom ($Z = 80$), the Schiff shielding effectively suppresses the applied electric field by a factor of order 3×10^{-4} . Heavy atoms are better than light ones because of the factor Z^2 , which is due to the enhanced electron density near a highly charged nucleus. A more careful calculation shows that there is an additional relativistic enhancement factor K_r , which can be as large as 10 for heavy atoms, (Khriplovich 1991) but that is beyond the scope of this lecture.

Why a Molecule is Better

A molecule can be much more sensitive than an atom because $a_s a_p$ can be much larger. The s and p atomic orbitals of a polar molecule are strongly mixed since the atoms are highly polarized along the internuclear axis $\hat{\lambda}$. Without any external electric field \vec{E}_{ext} , the molecular rotation averages $[\vec{\nabla}^2 V]_0$ to zero, but it is easy to apply enough field to polarize $\hat{\lambda}$ completely in a heavy molecule. Taking $a_s a_p \sim 0.1$ as a typical value, Eq. (1.15) gives $[\vec{\nabla}^2 V]_0 \sim 0.4 Z^2 \hat{\lambda}$ (a.u.) independent of E_{ext} once it is sufficiently strong. The same quantity in an atom is $4Z^2 \vec{E}_{\text{ext}}$, which means that the Schiff interaction of a molecule is larger by a factor $1/(10E_{\text{ext}})$ (a.u.) or

$$\frac{\langle H^1 \rangle_{\text{molecule}}}{\langle H^1 \rangle_{\text{atom}}} \sim \frac{5 \times 10^8}{E_{\text{ext}}} \quad (1.22)$$

where E_{ext} is the field in V/cm applied to the atom. For a typical field of 5kV/cm this is a factor of 10^5 , quite an improvement in sensitivity!

LECTURE 2

The TIF experiment on nuclear spin dependent T-violation

A. Possible Origins of T-Violation

In lecture 1 we discussed the discrete symmetries C, P, and T, and saw that the existence of an EDM in an elementary system such as a neutron, atom, or molecule would imply the violation of T-symmetry in nature. One might crudely divide the possible origins of the T-violations into the following categories: (i) nucleon-nucleon interactions or intrinsic nucleon EDM, (ii) electron-electron interactions or intrinsic electron EDM, and (iii) electron-nucleon interactions. The first of them is characterized by the Schiff moment, as we saw in lecture 1, and corresponds to an interaction of the form $\hat{\sigma}_N \cdot \hat{\lambda}$ where $\hat{\sigma}_N$ is along the nuclear spin, and $\hat{\lambda}$ is a polar axis associated with the (shielded) applied electric field. The second gives rise to a $\hat{\sigma}_e \cdot \hat{\lambda}$ interaction, where $\hat{\sigma}_e$ is along the electron spin, as we will discuss more fully in lecture 4. Interactions of the third type can give rise both to a nuclear spin dependent interaction $\hat{\sigma}_N \cdot \hat{\lambda}$ and to an electron spin interaction $\hat{\sigma}_e \cdot \hat{\lambda}$.

The simplest suitable electron-nucleon interaction we can postulate is the neutral-current weak interaction

$$H_{P,T} = i \frac{G_F}{\sqrt{2}} (C_T \bar{n} \sigma^{\mu\nu} n \bar{e} \gamma_5 \sigma_{\mu\nu} e + C_S \bar{n} n e \gamma_5 e). \quad (2.1)$$

Here we are using an effective 4-fermion interaction (Commins and Bucksbaum 1983), which is suitable only in our low-energy atomic context. The scale of the interaction is characterized by G_F the Fermi coupling constant, which has the value 2.2×10^{-14} a.u.. The first term, known as the tensor-pseudotensor interaction (since $\sigma^{\mu\nu}$ is the Lorentz-invariant tensor constructed from Dirac matrices), is characterized by a constant C_T and reduces in the non-relativistic limit to the effective interaction $\hat{\sigma}_N \cdot \hat{\lambda}$. The second term, the scalar-pseudoscalar interaction, corresponds to $\hat{\sigma}_e \cdot \hat{\lambda}$ and is characterized by C_S . More details of weak interaction theory can be found in (Commins and Bucksbaum 1983). The point I am making here is that C_T describes the strength of the T-violating weak interaction that gives a $\hat{\sigma}_N \cdot \hat{\lambda}$ effective coupling. $C_T=1$ means it is as strong as the normal weak interaction. Similarly C_S characterizes the weak interaction that gives a $\hat{\sigma}_e \cdot \hat{\lambda}$ coupling.

Some experiments search for T-violation associated with nuclear spin, while others look for effects connected with electron spin. The former determine the nuclear Schiff moment Q and the weak interaction constant C_T . From Q one obtains information about the nucleon-nucleon interactions and the intrinsic nucleon EDMs, which can, in turn, be related to the constituent quarks and gluons. The latter give information about C_S and the electron EDM.

Current experiments

At the forefront of sensitivity to the nuclear spin dependent EDM there are three experiments in close competition, involving the neutron (Golub and Lamoreaux, 1994), the ^{199}Hg atom (Jacobs et al. 1993), and the molecule ^{205}TlF (Cho et al. 1991). In the rest of this lecture we will describe the TlF experiment and its results. The most sensitive of the experiments to detect an electron spin dependent interaction involve the atoms Tl (Commins et al. 1994) and Cs (Murthy et al. 1989). We are planning a new electron-spin experiment using the paramagnetic molecule YbF, which will be discussed in lecture 4.

B. The TlF Experiment

a) Principle of the experiment

The experiment (Cho et al. 1991) involved the spin-polarized TlF molecule, placed in an electric field \vec{E}_{ext} . Nuclear magnetic resonance (NMR) was performed on the Tl nucleus and we looked for a linear Stark effect by searching for a shift of the NMR frequency when \vec{E}_{ext} was reversed. The interaction of the Tl nuclear spin $(1/2)\hbar\vec{\sigma}$ with the rest of the molecule can be described by the effective Hamiltonian

$$H = -\mu_{\text{Tl}}\hat{\sigma} \cdot \vec{B}_0 - dh\hat{\sigma} \cdot \hat{\lambda}. \quad (2.2)$$

The first term is the usual (T-conserving) hyperfine interaction of the nuclear magnetic dipole moment $\mu_{\text{Tl}}\hat{\sigma}$ with the internal magnetic field \vec{B}_0 of the molecule. The second term describes the P&T-violating electric dipole interaction that we are interested in. Here $\hat{\lambda}$ is a unit vector pointing from the Tl nucleus to the F nucleus, d is a measure of T-violation in TlF and h is Planck's constant. In free space, such an interaction would tip the internuclear axis, giving it a small projection along $\vec{\sigma}$, hence producing a small permanent EDM. We prefer, however, to detect this interaction by applying the strong field \vec{E}_{ext} , which substantially polarizes $\hat{\lambda}$, and to look for an energy of the form $\vec{\sigma} \cdot \vec{E}_{\text{ext}}$ as discussed in lecture 1. This energy appears as a shift of the NMR frequency when \vec{E}_{ext} is reversed.

A schematic view of the experiment is shown in fig. 1. A beam of molecules was produced by a supersonic jet source. The temperature of the molecules was sufficiently low that they were all in the electronic ground state and most of them were in the vibrational ground state ($^1\Sigma, v = 0$), however, a large number of rotational and hyperfine states were occupied. Our measurement was performed using only one particular magnetic hyperfine sublevel of the first excited rotational state $J=1$.

Within $J=1$ there are twelve magnetic sublevels corresponding to the three projections of $|J = 1\rangle$ and the two projections of each spin-1/2 nucleus. In order to select a particular one of these, we used the combination of an electrostatic quadrupole lens together with a so-called state selector. First, the lens focussed those molecules having $(J = 1, M_J = 0)$ and deflected the $M_J = \pm 1$ molecules out of the beam. Next, the four nuclear spin states were resolved in the state selector by a 27 G magnetic field, B_{ext} , and an oscillating field drove a transition (schematically shown as A in fig. 2.1) from one of these four states to one of the eight sublevels in the manifold $(J = 1, M_J = \pm 1)$. These selected molecules were the ones on which our measurement was made. The Tl nuclear spin transition (labeled C in fig. 2.1) was induced in them using separated oscillating magnetic fields to produce a narrow Ramsey resonance line. Finally, a second combination of state selector (transition B) and electric quadrupole rendered the NMR transition observable: it focussed the beam onto a hot wire detector when $\hat{\sigma}$ was unchanged but defocussed it when $\hat{\sigma}$ had been flipped.

b) The Ramsey Resonance

Figure 2.2 shows the eight sublevels of the manifold $(J=1, M_J \neq 1)$ in high electric field E_{ext} , together with their magnetic quantum numbers $(M_J = \pm 1, M_{\text{Tl}} = \pm \frac{1}{2}, M_{\text{F}} = \pm \frac{1}{2})$. The NMR transition that we excited was one of the Tl nuclear spin flips; either $J \rightarrow E$ or $K \rightarrow H$ depending upon the state chosen by the state selectors. Since levels J and K are degenerate, as are E and H, (they differ only in the signs of the magnetic quantum numbers) the two transitions are resonant at the same frequency $f_0 = 119.57\text{kHz}$ at $E_c = 29.5\text{kV/cm}$.

The transition was driven by a pair of separated oscillating magnetic fields of frequency f whose relative phase was switched under computer control between $\pm\pi/2$. The difference signal, plotted as a function of frequency, produced the antisymmetric Ramsey lineshape [21] shown in fig. 2.3. Near the center of the line this difference signal is well characterized by

$$S = I_0 \sin[2\pi T(f - f_0)], \quad (2.3)$$

where I_0 is the peak number of molecules per second in the resonance signal and T is the time of flight between the two separated oscillating fields.

c) Reversals

Now we turn to the three main reversals employed in our experiment. The first of these was a reversal of the sign of the electric field \vec{E}_{ext} . This reversed the polarization of the molecule $\langle \hat{\lambda} \rangle$ but did not affect any of the angular momenta and, in accordance with Eq. (2.2), produced a shift of $-4d|\langle \vec{\sigma} \cdot \hat{\lambda} \rangle|$ in the resonance frequency. We looked for the corresponding change in the signal S , given by Eq. (2.3). Note that electric field reversal is similar to performing a parity transformation. In order to approximate this as closely as possible in our experiment, we reversed all the electric fields in the apparatus, i.e. state selector and quadrupole fields as well as \vec{E}_{ext} . Ideally one might also have hoped to reverse the beam velocity, but this was not done.

Our second main reversal was to change the sign of the magnetic fields in the state selectors. Since the state selector resonance populated a specific magnetic sublevel (either J or K) relative to the direction of the field, this modulation reversed the signs of all the chosen angular momenta relative to an axis fixed in the laboratory. In the language of Eq. 2.2, this corresponded to a reversal of the T1 spin $\hat{\sigma}$ and of the internal magnetic field \vec{B}_0 . Consequently it produced the same frequency shift as reversal of E_{ext} , but by an experimentally independent method. Note that this reversal of the angular momenta and magnetic fields was very similar to a time reversal transformation although, again, we did not reverse the beam velocity.

The third primary modulation also allowed us to reverse the magnetization state of the molecule but this time without changing the state selector magnetic fields. This was accomplished by changing the frequency of the rf fields in the state selectors.

d) Results and their Implications

The shift of the resonance frequency that was properly synchronous with all these reversals gave the experimental result

$$d = -0.13 \pm 0.22 \text{ mHz} \quad (2.4)$$

for the T-violating coupling constant in Eq. (2.2). In order to extract a Schiff moment for the T1 nucleus from this result, it is necessary to calculate the electronic integral $\langle \vec{\nabla} \nabla^2 V \rangle$, as we discussed in lecture 1. This calculation has been done by Coveney and Sandars (1983) and when combined with our measurement of d gives

$$Q_{Tl} = (2.3 \pm 3.9) \times 10^{-10} \text{ e.fm}^3. \quad (2.5)$$

The experiment on atomic ^{199}Hg (Jacobs et al. 1993) measures an upper limit on the Schiff moment of that nucleus,

$$|Q_{\text{Hg}}| \leq 0.3 \times 10^{-10} \text{ e.fm}^3, \quad (2.6)$$

while the most recent neutron EDM measurement yields

$$d_n = (-3 \pm 5) \times 10^{-13} \text{ e.fm}. \quad (2.7)$$

These are small limits indeed: for example, the dipole distortion of the neutron is less than 10^{-12} of its diameter.

The experimental result in Eq. (2.4) can also be used to determine the weak electron-nucleon coupling constant C_T discussed in section A of this lecture:

$$C_T = (-2 \pm 3) \times 10^{-7}, \quad (2.8)$$

and an even stronger limit comes from the experiment on ^{199}Hg

$$|C_T| < (0.2) \times 10^{-7}. \quad (2.9)$$

It is interesting to compare this atomic physics limit with the only known T-violating weak interaction effect, namely the CP-violating K_L^0 decay, where the effective weak interaction strength 2×10^{-3} . These measurements of C_T show that the T-violating electron-nucleon interaction is five orders of magnitude smaller than that.

When the experimental limits given above are used to limit possible T-violating elementary particle interactions, the exact sensitivity of each experiment to a given hypothetical effect depends upon the details of the effect. However, the general trend is that the neutron gives the strongest limit, followed closely by Hg, while the TIF constraint is typically a factor of ten weaker than the neutron. It is nevertheless important to make measurements in several different systems because the nature and extent of T-violation is completely uncertain at present and such studies provide an excellent prospect for learning something new about physics beyond the standard model.

LECTURE 3

Aharonov-Bohm and Aharonov-Casher Phases

We leave the subject of T-violation for a moment to discuss a recent experiment on the Aharonov-Casher phase performed by Sangster et al. (1993, 1995) using the TIF molecular beam.

A. Geometric Phases

a) The Aharonov-Bohm Effect

When a particle propagates along some path P_1 , its wavefunction acquires a phase factor $\exp(iS/\hbar)$ where S is the action along that path. If the particle is charged and there is an electromagnetic potential (ϕ, \vec{A}) along the path then

$$S_{P_1} = q \int_{P_1} -\phi dt + \vec{A} \cdot d\vec{x} \quad (3.1)$$

is the part of the action associated with the electromagnetic interaction. In many cases, this phase factor is of no physical interest, but if there are two significantly different paths P_1 and P_2 between the same initial and final state, then the final state exhibits interference fringes depending on the phase difference $(S_{P_2} - S_{P_1})/\hbar$ between the two paths. This was first pointed out by Aharonov and Bohm (1959).

Fig. 3.1 shows two schemes for realizing the Aharonov-Bohm (AB) effect. In the first, the particle passes through a beam splitter and into two long conducting cylinders. While it is inside the cylinders, a potential difference $\phi(t)$ is turned on and then turned off. The particle exits and the two paths are brought together on a second beam splitter. According to Eq. (3.1) the phase difference between the two paths has an electromagnetic part $-\frac{q}{\hbar} \int \phi(t) dt$ which can be varied to produce interference fringes in the final state probability. Fig. 3.1 also shows a magnetic version in which the two paths encircle a long solenoid, and the phase difference $\frac{q}{\hbar} \oint \vec{A} \cdot d\vec{x}$ controls the final state. These are known as the scalar and vector AB effects. The vector effect has been studied experimentally (Tonomura et al. 1982) but the scalar one has not.

The interesting point about these experiments is that the trajectory of the particle leaving the final beam splitter can be altered by varying ϕ or A , even though there is no force acting on it at any time. A further interesting aspect of the vector effect is that the path integral $\oint \vec{A} \cdot d\vec{x}$ is just equal to the enclosed flux and therefore does not depend on any details of the path. Since any path of this geometry gives the same result, this is sometimes called a geometric phase. Finally, we remark that the division between scalar and vector contributions is rather arbitrary because each transforms into the other according to the velocity of the observer. It is worth noting that the phase given by Eq. (3.1) can be rewritten in terms of the 4-vectors (A^0, \vec{A}) and (x^0, \vec{x}) as $-\frac{q}{\hbar} \int A^\mu dx_\mu$. In this form it is evident that the phase of the interference pattern is invariant under Lorentz transformations, as indeed it must be.

b) The Aharonov-Casher Effect

Neutral particles do not exhibit the Aharonov-Bohm effect because their charge is zero. However the magnetic dipole moment $\vec{\mu}$ couples to electromagnetic fields, resulting in phase shifts and interference effects that are analogous. These were first discussed by Aharonov and Casher (1984). The phase associated with this coupling can be written

$$\Phi = \frac{1}{\hbar} \int -\vec{\mu} \cdot \vec{B} dt + \frac{1}{c^2} \vec{\mu} \times \vec{E} \cdot d\vec{x}. \quad (3.2)$$

Fig. 3.2 shows two schemes for realizing the Aharonov-Casher (AC) effect. The first probes the scalar part by applying a magnetic field to one arm of the interferometer so that the final state of the particle is determined by the phase shift $-\frac{1}{\hbar} \int \vec{\mu} \cdot \vec{B} dt$. This analog of the scalar AB effect has been studied by Allman et al. (1993). The second scheme demonstrates the vector effect, using a line charge to produce an electric field and hence a phase difference $\frac{1}{\hbar c^2} \oint \vec{\mu} \times \vec{E} \cdot d\vec{x}$. If $\vec{\mu}$ is always perpendicular to the plane of the path¹, this integral is just proportional to the strength of the line charge and independent of the exact path. In this respect it seems to be geometric, like the AB phase. An important difference, however, is that the flux enclosed by a loop is well-defined, whereas the enclosed line charge is defined only if the charge per unit length is uniform. Thus the vector AC phase is geometric only when we restrict ourselves to a uniform line charge and a magnetic moment perpendicular to the path.

¹ More precisely, the condition is that the component of $\vec{\mu}$ along $\vec{E} \times d\vec{x}$ be constant over the path.

As we have already mentioned, part of the appeal of the AB effect is that one can arrange to have no forces exerted on the particle. This can also be accomplished in the AC case. For the scalar effect, one only needs to turn the solenoid on and off while the particle is inside, where the field is uniform. The question of forces in the vector case is much more subtle, but after substantial discussion in the literature it seems that there is no force in this case either (Aharonov et al. 1988). The primary difference between the AB and the AC effects is that the former involves an electromagnetic potential acting on a charge, while in the latter it is a field which couples to a dipole moment. From one point of view, this seems to make the Aharonov-Bohm effect more interesting since we are used to thinking that fields act on particles while potentials are just mathematical abstractions. However, the AC case is no less mysterious since there are still no forces acting on the particle and yet its final trajectory can be altered by changing the fields.

B. Measurement of AC Phase

a) Principle of experiment

In the rest of this lecture, I discuss the experimental verification of the vector AC phase. It was first tested in a neutron interferometer (Kaiser et al. 1991; Cimmino et al. 1989), where the measured phase shift was 2.11 ± 0.34 mrad, compared with the predicted value of 1.52 mrad. Although the observed phase was nearly two standard deviations above the theoretical value, the experiment did seem to confirm the existence of the effect. However, there was no experimental verification of the two most notable features, velocity-independence and proportionality to electric field. Subsequently, there were suggestions for observing the AC effect in similar interferometers using atoms instead of neutrons (Kasevich and Chu 1991; Keith et al. 1991), but the first results using atoms and the first tests of the velocity- and field-dependence were obtained by a different technique in our laboratory (Sangster et al. 1993, 1995) using the TIF beam.

The scheme shown in Fig. 3.3(a) involves two coherent beams with the *same* magnetic moment traveling on *different* paths around a charged wire. The beam on path *a* acquires an AC phase shift

$$\Phi_a = \frac{1}{\hbar c^2} \int \vec{\mu} \times \vec{E}(\vec{r}_a) \cdot d\vec{r}_a. \quad (3.3)$$

A similar expression applies to path *b*, and the net accumulated phase difference is $\Delta\Phi = \Phi_a - \Phi_b$.

It is not necessary for the paths a and b to enclose a line of charge in order to observe the AC effect. Sangster et al. (1993) have pointed out another possible configuration, shown in Fig. 3.3(b), where the two coherent beams have *different* magnetic moments (μ_a and μ_b) and are not spatially separated; they pass through the *same* electric field. In this arrangement the AC phase shift between the two arms of the interferometer is given by

$$\Delta\Phi_{AC} = \frac{1}{\hbar c^2} \int (\vec{\mu}_a - \vec{\mu}_b) \times \vec{E} \cdot d\vec{r}. \quad (3.4)$$

For simplicity we assume as shown in Fig. 3.3(c) that the beam travels a distance L on a path along the y axis and that \vec{E} lies in the z direction, then the x component of the magnetic moment is the only relevant one, and

$$\Delta\Phi_{AC} = \frac{1}{\hbar c^2} ([\mu_x]_a - [\mu_x]_b) EL. \quad (3.5)$$

The loop corresponding to the two paths in the interferometer does not now enclose any line charge and therefore appears different from the situation considered by Aharonov and Casher. In order to obtain a non-vanishing path integral we have taken advantage of the fact that $\vec{\mu}$ in Eq. (3.3) need not be fixed with respect to $\vec{E} \times d\vec{r}$. It is worthwhile to note, however, that path a of Fig. 3.3(b) can be continuously deformed at constant $\Delta\Phi_{AC}$ to recover the geometry of Fig. 3.3(a) by passing over the end of the line charge or, if it is infinitely long, through an infinitesimal cut in the line. This is possible because the AC phase is not geometric, except when the direction of μ is constrained as discussed in section 3.A.b.

It is by no means necessary to use neutrons, any neutral particle with a magnetic moment should exhibit the AC effect; all that is required is a convenient way of preparing the magnetic moment in a coherent superposition of two states with different values of μ_x and detecting the accumulated AC phase difference. We have chosen to use Ramsey's method of separated oscillatory fields (Ramsey 1956), in which the first field prepares a coherent superposition of two spin states ($[\mu_x]_a$ and $[\mu_x]_b$) and the second probes the phase that has evolved between them. Thus the experiment involves magnetic resonance in the presence of an electric field. When the electric field polarity is reversed, the sign of the AC phase changes and this appears as a phase shift of the Ramsey resonance line.

We observed the AC phase using the fluorine nuclei in our TIF molecular beam in a strong (10-30 kV/cm) external electric field \vec{E} . As in the experiment of lecture 2, the molecules were in the electronic and vibrational ground states $^1\Sigma^+$, $v=0$, and in the first excited rotational state $J=1$. The rotational states are strongly mixed by the applied electric field, so J is not a good quantum number, but it serves adequately to identify which rotational state we use. Within the $J=1$ manifold there are twelve hyperfine sublevels corresponding to the magnetic quantum numbers of the rotation ($M_J = 0, \pm 1$), Tl nuclear spin ($M_{\text{Tl}} = \pm \frac{1}{2}$), and F nuclear spin ($M_{\text{F}} = \pm \frac{1}{2}$). In a strong electric field, these separate into four $M_J = 0$ and eight $M_J = \pm 1$ states, the latter being shown in fig 2.2. The transitions studied in this experiment, were F-H and I-K, which correspond closely to simple flips of the fluorine nuclear spin.

Using the state selector described in lecture 2, we first prepared the molecules in the initial state a ($a = \text{F or I}$). The beam then passed through the first of two Ramsey loops in which an rf magnetic field near-resonantly excited a coherent superposition of the states a and b ($b = \text{H or K}$) with roughly equal amplitudes. This loop was effectively the beam splitter of our interferometer, providing the required coherent superposition of magnetic moments μ_a and μ_b . The molecules traveled in this state for a distance L before reaching the second rf loop which played the role of the re-combining beam splitter. The rest of the apparatus then determined what fraction P of the molecules made the transition from a to b . Close to resonance, the Ramsey fringe pattern has the usual form

$$P = \frac{1}{2} \left[1 + \cos \left((\omega - \omega_0) \frac{L}{v} + \delta + \Delta\Phi \right) \right] \quad (3.6)$$

where ω is the rf frequency, ω_0 is the resonance frequency, v is the beam velocity, δ is the phase difference between the two rf fields, and $\Delta\Phi$ is any additional phase shift between the two states a and b in the interferometer, such as the AC phase.

Since the molecule in external electric field is cylindrically symmetric around the field direction z , the expectation value of the transverse magnetic moment μ_x is zero in any of these states. It follows from Eq. (3.5) that the AC effect is completely suppressed. While this is a great advantage in the search for an EDM, where the AC effect is a potential source of systematic error, it is obviously an obstacle to be overcome in the present context. In order to study the AC phase, we must rotate

the magnetic symmetry axis so that the magnetic moment of the molecule can have a nonzero projection μ_x . This was done by applying a uniform magnetic field \vec{B} along the x axis, as shown in Fig. 3.3(c).

To summarize, the experiment involved a radiofrequency transition between two hyperfine sublevels a and b of the TIF molecule, which are separated in energy by $\hbar\omega_0$. A magnetic field B_x induced transverse magnetic moments $[\mu_x]_a$ and $[\mu_x]_b$, and a strong electric field E_z produced an AC phase shift between the two levels (in addition to the usual $\omega_0 t$ due to the energy difference between the levels). When either applied field was reversed, the AC phase changed sign, allowing us with the help of Eq. (3.6) to deduce $\Delta\Phi$ from the measured changes in the transition probability P . This experimental phase shift could be compared with a theoretical prediction (based on Eq. (3.5) together with the calculated value of $[\mu_x]_a - [\mu_x]_b$) in order to test the validity of the theory. Details about the calculation of the transverse moments $[\mu_x]_a$ and $[\mu_x]_b$ are beyond the scope of these lectures but can be found in Sangster et al. (1995).

b) Experimental Results

The AC phase shift $\Delta\Phi_{AC}$ was picked out by the fact that $\mu \times \vec{E}$ changes sign when either E_z or B_x is reversed. This allowed us to use a form of phase-sensitive detection in which we looked for a phase shift of the Ramsey fringes in synchronism with reversals of E_z and B_x . At the central zero-crossing of the Ramsey pattern, a small phase shift appeared as a proportional change in the number of molecules hitting the detector. In order to convert this change in count rate to an equivalent frequency shift, we made an on-line measurement of the derivative of the resonance signal with respect to frequency at the zero-crossing. Since the frequency interval between zero-crossings corresponds to a phase shift of π , the equivalent frequency shift could finally be converted to a measured AC phase shift.

The molecular beam was focused by two electrostatic quadrupole lenses, whose focal lengths depend upon the strength of the quadrupole field and on the velocity of the molecules. Thus our resonance signal was derived from a narrow slice ($\sim 20\%$) of the full Maxwell Boltzmann distribution, which we were free to choose by adjusting the voltages on the quadrupole lenses. The velocity was measured by the fringe spacing of the Ramsey pattern, which goes through zero each time the quantity $(\omega - \omega_0)/v$ increases by π , as can be seen from Eq. 3.6.

We set the magnetic field B_x to a value (approximately 1.3 G) such that the resonance of the I-K transition increased from 22.1677(3) kHz to 22.70(1) kHz. Knowing this frequency shift, we were able to calculate $[\mu_x]_a - [\mu_x]_b$, as described by Sangster et al. (1995). The potential difference across the electric field plates was set to 20.1(1)kV/cm. Knowing that the spacing between the rf coils was $L=2.066(5)$ m, we used Eq. (3.5) to predict a value for the AC phase of 2.47(2) mrad, shown as the solid line in Fig. 3.4. In the same figure, we also show the phases measured at seven different velocities ranging from 188 m/s to 366 m/sec. The weighted mean of the experimental points is 2.42(5) mrad in excellent agreement with the theoretical expectation. We see no evidence for any deviation from the predicted velocity-independence.

Next, the velocity was fixed at 254 m/sec while the electric field was varied from 5-20 kV/cm, as shown in Fig. 3.5. The theoretical prediction, shown once again by a solid line, is not quite linear in E_z due to a small Stark shift of the resonance. The experimental points show the AC phase measured at four different values of the electric field, approximately 5, 10, 15, and 20 kV/cm. Again, there is no evidence of any discrepancy between theory and experiment.

The most stringent check of the theory is obtained by dividing the value of each measured phase by the corresponding predicted value. A weighted average over all the points we measured using the 2-3 transition gives

$$\frac{\Delta\Phi_{\text{exp}}}{\Delta\Phi_{\text{th}}} = 0.98(2) \quad (3.7)$$

An earlier experiment using the F-H transition also confirmed the theory but with less precision (Sangster et al. 1993).

c) Conclusions

In this lecture we have studied the AC phase, which is an analogue found in neutral, spin-1/2 particles of the AB phase for charged particles. We have shown that although it may share some of the geometric features of the AB phase, this phase can be observed without requiring that the particles encircle a line charge. Finally, we have outlined an experiment to measure the phase shifts actually exhibited by molecules moving in an electric field, which shows that they are accurately described by the AC effect at the 2% level.

LECTURE 4

Searching for the electron EDM

A. Schiff's Theorem and the electron EDM

We return now to the main theme of these lectures - the search for T-violation in atomic and molecular systems. In lectures 1 and 2 we focussed on T-violating effects proportional to nuclear spin (characterized by the Schiff moment Q and the weak tensor coupling C_T) and we discussed the finite nuclear size as a mechanism for avoiding Schiff's theorem. The volume effect does not work for electrons because they are point particles but as you may recall from lecture 1, relativistic effects provide another mechanism. If an atom is sufficiently heavy, the electrons can be quite relativistic and if they have an EDM it can lead to significant atomic EDM effects.

We take as our zeroth order Hamiltonian the Dirac equation

$$H^0 = \sum_{\text{electrons}} \beta m c^2 + \vec{\alpha} \cdot c \vec{p} + V, \quad (4.1)$$

where V includes the uniform applied field \vec{E}_{ext} as well as the atomic Coulomb interaction. Now we would like to let the electron have an EDM d and to treat the electric dipole interaction as a perturbation, but what is the correct relativistic form of the interaction? The *magnetic* dipole interaction for a spin-1/2 particle of magnetic moment μ can be introduced into the Dirac equation by a term (Bjorken and Drell 1964) $H_{M1} = \frac{\mu}{2} \sigma_{\mu\nu} F^{\mu\nu}$, where $\sigma^{\mu\nu}$ is the tensor $\frac{i}{2} [\gamma^\mu, \gamma^\nu]$ and $F^{\mu\nu}$ is the electromagnetic field. Following Salpeter (1958) we take it that the *electric* dipole interaction is just the odd-parity counterpart $\gamma_5 H_{M1}$. That is, we take

$$H_{E1} = \frac{d}{2} \gamma_5 \sigma_{\mu\nu} F^{\mu\nu}, \quad (4.2)$$

where d is the supposed EDM of the electron. Converting from covariant notation to Dirac notation, the interaction becomes

$$H_{E1} = -d\beta(\vec{\sigma} \cdot \vec{E} + ic\vec{\alpha} \cdot \vec{B}). \quad (4.3)$$

Here β , $\vec{\sigma}$ and $\vec{\alpha}$ are the standard Dirac operators. To be concrete, let us choose the representation

$$\beta = \begin{bmatrix} 1 & 0 \\ 0 & -1 \end{bmatrix}, \quad \vec{\sigma} = \begin{bmatrix} \hat{\sigma} & 0 \\ 0 & \hat{\sigma} \end{bmatrix}, \quad \vec{\alpha} = \begin{bmatrix} 0 & \hat{\sigma} \\ \hat{\sigma} & 0 \end{bmatrix}, \quad (4.4)$$

$\hat{\sigma}$ being the Pauli matrix. The familiar classical expression $-\vec{d} \cdot (\vec{E} + \vec{v} \times \vec{B})$ is the non-relativistic limit of this interaction. In atoms and molecules with an unpaired electron, the electric term in Eq. (4.3) is much larger than the magnetic one, so we take as our perturbation

$$H^1 = -d\vec{\sigma} \cdot \vec{E}. \quad (4.5)$$

Notice the important difference between this and the non-relativistic operator, namely, the factor β . In a heavy atom we should really sum over electrons, but to keep the notation simple I will not write a \sum sign. The EDM interaction energy of the atom is therefore

$$\langle H^1 \rangle = \langle \psi^0 | -d\vec{\sigma} \cdot \vec{E} | \psi^0 \rangle. \quad (4.6)$$

The total field \vec{E} on the electron can be written as $-\vec{\nabla}V/q$ where V is the potential in Eq. (4.1). From this it follows (Sandars 1965) that

$$\vec{\sigma} \cdot \vec{E} = -[\vec{\sigma} \cdot \vec{\nabla}, H^0/q], \quad (4.7)$$

where H^0 is the relativistic Hamiltonian of Eq. (4.1). But this commutator vanishes, which means that $\langle \psi^0 | d\vec{\sigma} \cdot \vec{E} | \psi^0 \rangle = 0$, i.e. the nonrelativistic interaction vanishes in accordance with Schiff's theorem. Finally, since this matrix element is zero, we can add it to the right-hand side of Eq. (4.6) to obtain

$$\langle H^1 \rangle = \langle \psi^0 | (1 - \beta)d\vec{\sigma} \cdot \vec{E} | \psi^0 \rangle, \quad (4.8a)$$

which can be written explicitly as

$$\langle H^1 \rangle = \left\langle \psi^0 \left| \begin{array}{cc} 0 & 0 \\ 0 & 2d\hat{\sigma} \cdot \vec{E} \end{array} \right| \psi^0 \right\rangle. \quad (4.8b)$$

This form of the interaction energy obviously satisfies Schiff's theorem since it only couples to the small components of the wavefunction and therefore vanishes in the nonrelativistic limit.

Since the integral in Eq. (4.8) is dominated by the region very close to the nucleus, where the electron is moving fast, the total field \vec{E} on the electron can be reasonably approximated by $Ze\hat{r}/r^2$, the Coulomb field near the nucleus. Writing the two small components of $|\psi^0\rangle$ as $|g^0\rangle$, we obtain the approximation

$$\langle H^1 \rangle = \left\langle g^0 \left| 2d\hat{\sigma} \cdot \frac{Ze\hat{r}}{r^2} \right| g^0 \right\rangle. \quad (4.9)$$

This vanishes unless g^0 is a state of mixed parity (because \hat{r} is an odd-parity operator), which means that the interaction requires the external field \vec{E}_{ext} . Let us expand the small component of the wavefunction in angular momentum eigenstates, just as we did for the non-relativistic wavefunction in lecture 1. The small components of $p_{1/2}$ and $s_{1/2}$ states have orbital angular momenta $l=0$ and 1 respectively, so the leading terms are

$$g^0 = a_p g_{p_{1/2}} + a_s g_{s_{1/2}} + \dots \quad (4.10)$$

Once again, the higher angular momentum functions are suppressed at the origin and $\langle H^1 \rangle$ comes largely from these two leading terms. As a result, one finds in atomic units (the details are in Khriplovich's book (1991))

$$\langle H^1 \rangle \approx 8a_s a_p (Z\alpha)^2 Z d\hat{\sigma} \cdot \hat{\lambda}. \quad (4.11)$$

Here the factor $(Z\alpha)^2$ is due to the size of the small components of the wavefunction, Z is due to the Coulomb field, and $\hat{\lambda}$ is the axis of the s-p mixing. For an atom we estimate once again that $a_s a_p \hat{\lambda} \sim \vec{E}_{\text{ext}}$ (see Eq. (1.20) and the associated text). Then putting $Z = 70$ into Eq. (4.11) we find that

$$\langle H^1 \rangle_{\text{Atom}} \sim 100 d\hat{\sigma} \cdot E_{\text{ext}}, \quad (4.12)$$

which means that in spite of Schiff's theorem, the EDM interaction in a heavy atom is 100 times larger than that of the free electron! This marvelous enhancement factor was first noticed by Sandars (1965).

The situation in a polar molecule is even more favorable since we can have $a_s a_p \hat{\lambda} \sim 0.1$ along the external field. In that case

$$\langle H^1 \rangle_{\text{molecule}} \sim 10 d\hat{\sigma} \cdot \hat{\lambda}, \quad (4.13)$$

which is larger by a factor $\sim 5 \times 10^8/E_{\text{ext}}$ than the atomic interaction. This additional enhancement of a molecule relative to an atom is exactly the same as the factor we encountered in lecture 1 in the context of the Schiff interaction, namely the large mixing of s and p orbitals in a polar molecule. Our conclusion is that if the electron has an EDM, the effect in a heavy polar molecule should be similar to that of the free electron in a field of $10 \text{ au} = 5 \times 10^{10} \text{ V/cm}$. This is a huge effective electric field.

B. Suitable Molecules

Our discussion of suitable molecules is restricted to diatomics because the spectra for polyatomic systems are so much more complex. Candidates of interest should be polar (for large $a_s a_p$), heavy (for large $Z^3 \alpha^2$) and paramagnetic (since the interaction depends on $\hat{\sigma}$). We also need to be able to polarize the molecule fully along the external field \vec{E}_{ext} , so the rotational states should not be too widely split. Taking the molecular dipole to be $\mu_e \sim e a_0$ and the external field to be $< 50 \text{ kV/cm}$, this places an upper limit on the rotational constant B of about 1^{-1} cm , which excludes the hydrides. The heaviest candidates, such as NpO or RaF, for example, are not very appealing because they are radioactive and cannot easily be handled in large amounts. There are a number of heavy but stable oxides and sulfides, such as ThN, LuO, and BiS but these tend to have very low vapor pressure and would involve working with extremely hot sources.

We do not discuss all the possibilities here, but go instead to the most promising group, the fluorides. Table 4-1 lists some of the heavier ones, together with some relevant information. From the standpoint of intrinsic sensitivity, HgF seems to be the best, with an effective electric field of almost 10^{11} V/cm on the electron spin. However, there does not seem to be a convenient way to detect the molecule with high efficiency because the ionization energy of Hg is very high and the first optical transition to a bound state is in the uv at 256nm. The next most sensitive molecule is YbF, which can be detected both by a hot wire and by laser induced fluorescence. This makes it preferable to PbF which has a similar effective electric field on the electron EDM. Finally, BaF is an interesting case because it is very convenient to work with and the effective electric field, though not the largest, is still very large. These considerations have led us to try making an electron EDM measurement using YbF, and the rest of this lecture describes the current status of that attempt.

C. Progress with YbF

Yb is a transition element in the lanthanide group, but because the ground state configuration is $4f^{14}6s^2$, it is in many respects similar to an alkaline earth. One of the two 6s electrons bonds

ionically with the F atom, leaving a simple valence electron whose spectrum is very similar to that of an alkali. The ground state X is in a $^2\Sigma$ configuration, while the first excited state A is a $^2\Pi$. We find that a good way to produce a molecular beam of YbF is to heat YbF₃ and Al to ~1200°C in a zirconium crucible with a small hole in the lid. The resulting beam has been observed by means of an oxygenated rhenium hot wire and by laser induced fluorescence (LIF) on the $A^2\Pi_{1/2} - X^2\Sigma$ transition. In order to perform an electron EDM measurement, we need to know the resonance frequency for electron spin-flip transitions within the molecule, which means understanding the magnetic structure of the ground state.

For the most abundant isotope, ^{174}YbF , which has no Yb nuclear spin, the magnetic interaction Hamiltonian has the following structure

$$H = \gamma \vec{s} \cdot \vec{N} + b \vec{s} \cdot \vec{I} + c s_z I_z, \quad (4.14)$$

where \vec{s} is the electron spin, \vec{N} is the rotational angular momentum, \vec{I} is the F nuclear spin and the subscript z indicates projection along the internuclear axis. Since $s=1/2$ and $I=1/2$, there are four levels for each value of N , with relative energies determined by the constants γ , b and c . In the rotational spectrum, each transition of the P-branch ($\Delta N = -1$) is split into 4 lines by this structure, allowing us to determine the constants from the LIF spectra. Fig. 4.1 shows the P(70) and P(13) lines of the $A^2\Pi_{1/2} - X^2\Sigma$ transition measured by Sauer et al. [1995]. Although the laser is propagating at right angles to the molecular beam, there is some residual Doppler width (due to the divergence of the molecule beam) which is 15 MHz in the upper trace and 32 MHz in the lower. From a large number of such scans we were able to build up the map of ground-state energy levels versus the rotational quantum number N shown in fig. 4.2. Analysis of this map leads to the surprising conclusion that γ is very far from constant. In fact it is positive at low N , goes to zero at $N \sim 59$ and becomes negative at larger N . We find that the variation of γ is well described by the empirical formula

$$\gamma = \gamma_0 + \gamma_1 N(N+1) \quad (4.15)$$

in which $\gamma_0 = 13.31(8)$ MHz and $\gamma_1 = -3.801(15)$ kHz. A simple-minded estimate of γ_0 (as described by Sauer et al. 1995) gives $\gamma_0 \sim 270$ MHz, which is 20 times larger, whereas, the "centrifugal stretching" correction γ_1 is expected to be positive and at least 10 times smaller. This surprise has

yet to be explained quantitatively, but it seems likely that it is related to admixtures of the low-lying $4f^{13}$ configurations into the X and A states. Values were also obtained for the fluorine hyperfine constants: $b=142(2)\text{MHz}$, $c=84(8)\text{MHz}$.

As a result of this spectroscopy, we can now read off the ground state electron spin resonance frequencies as a function of N using fig. 4.2. Typically the frequency required is 100-200MHz. The basic experimental setup for an electron EDM experiment is illustrated in fig.4.3. The pump laser beam depopulates one of the four ground state levels by exciting A-X transitions. The two separated rf fields then drive an electron spin resonance which repopulates that level. Finally the probe laser, tuned to the same transition as the pump, excites laser-induced fluorescence in proportion to the rf resonance probability. The resonance will be studied in a strong external field \vec{E}_{ext} , which can be reversed in order to look for a frequency shift due to the electron EDM. We think it should be possible to detect shifts at the level of 1mHz, which means that an electron EDM as small as $10^{-28}e \cdot \text{cm}$ could be measured by this technique.

D. Connections with Particle Physics

Fig. 4.4 shows a history of electron EDM measurements. Each point represents a new upper limit on the electron EDM and shows the atomic system used to measure it. The lack of activity in the '70s and early '80s corresponds to a period of intense interest in P-violation without T-violation. During this time attention was focussed on testing the electroweak theory of Weinberg, Salam and Glashow (WSG) which predicted P-violation in atomic physics due to the neutral Z^0 particle. By 1986, the WSG model had become part of the standard model of elementary particle physics and parity violation was a well-established effect in atomic physics. There was then a resurgence of interest in T-violation because it provides a sensitive way to probe new interactions at much higher energy than the Z^0 mass, corresponding to effects in atoms that are much weaker than G_F . Since we do not know what physics lies at these energy scales, the EDM measurements provide important constraints on theory, even though they have so far been only upper limits. Figure 4.4 shows the range of electron EDM values expected in a few of the most popular extensions to the standard model and one sees that the measurements are entering the range where these theories start to be constrained. Theories predicting a larger electron EDM are not shown since they are, of course, already ruled out by the experiments. A detailed discussion about theories of elementary particle physics beyond the standard model is outside the scope of these lectures, but a number of

excellent reviews have been written on this subject, the most recent of which is by Barr 1993. This provides a clear explanation of the proposed theories and shows how they are tested by the parameters Q , C_T , d_e , C_s which we have discussed in these lectures.

REFERENCES

- Aharonov Y. and Bohm D., Phys. Rev. **115**, 485 (1959). The relationship between the Aharonov Bohm and Aharonov-Casher effects has been discussed by Aharonov and Casher 1984 and by C.R. Hagen, Phys. Rev. Lett. **64**, 2347 (1990).
- Aharonov Y., Pearle P., and Vaidman L., Phys. Rev. A **37**, 4052 (1988).
- Aharonov Y., Casher A., Phys. Rev. Lett. **53**, 319 (1984). See also Anandan J., Phys. Rev. Lett. **48**, 1660 (1982).
- Allman B.E., Cimmino A., Klein A.G., Opat G.I., Kaiser H., and Werner S.A., Phys. Rev. A **48**, 1799 (1993).
- Barr S.M., Int. J. Mod. Phys. A **8**, 209 (1993).
- Bjorken J.D. and Drell S.D., *Relativistic Quantum Mechanics* (McGraw-Hill, New York, 1964).
- Cho D., Sangster K., and Hinds E.A., Phys. Rev. A **44**, 2783 (1991).
- Christenson J.H., Cronin J.W., Fitch V.L., and Turlay R.J.H., Phys. Rev. Lett. **13**, 138 (1964).
- Commins E.D., Ross S.B., DeMille D., Regan B.C., submitted Phys. Rev. A 1994.
- Commins E.D. and Bucksbaum P.H., Weak Interactions of Leptons and Quarks, Cambridge University Press, (1983).
- Coveney P.V. and Sandars P.G.H., J. Phys. B: Atom. Mol. Phys. **16**, 3727 (1983).
- Golub R. and Lamoreaux S. K. Phys. Reports **237** 1 (1994).
- Jacobs J.P., Klipstein W.M., Lamoreaux S.K., Heckel B.R., Fortson E.N., Phys. Rev. Lett. **71**, 3782 (1993).
- Kaiser H., Werner S. A., Clothier R., Arif M., Klein A. G., Opat G.I., and Cimmino A., in Atomic Physics 12 edited by J. Zorn and R. Lewis (AIP, New York, 1991) p. 247. An earlier result of the same experiment was published by Cimmino A., Opat G.I., Klein A.G., Kaiser H., Werner S.A., Arif M. and Clothier R., Phys. Rev. Lett. **63**, 380 (1989).
- Kasevich M. and Chu S., Phys. Rev. Lett. **67**, 181 (1991). Keith D.W., Ekstrom C.R., Turchette Q.A., and Pritchard D.E., Phys. Rev. Lett. **66**, 2693, (1991).
- Khriplovich I.B., Parity Nonconservation in Atomic Phenomena, Gordon and Breach (1991).

Landau L., Nucl. Phys. **3**, 127 (1957).

Lee T.D. and Yang C.N., Phys. Rev. **104**, 254 (1956).

Murthy S.A., Krause D, Jr., Li Z.L., Hunter L.R., Phys. Rev. Lett **63**, 965 (1989).

Pauli W., Niels Bohr and the Development of Physics, Pergamon Press (1955).

Purcell E.M. and Ramsey N.F., Phys Rev. **78**, 807 (1950).

Ramsey N.F., Molecular Beams, (Oxford University Press, Oxford, 1956).

Salpeter E.E., Phys. Rev. **112**, 1642 (1958).

Sandars P.G.H., Phys. Lett. **14**, 194 (1965).

Sangster K., Hinds E.A., Barnett S.M., Riis E., and Sinclair A.G., submitted to Phys. Rev. A (1995).

Sangster K., Hinds E.A., Barnett S.M., and Riis E., Phys. Rev. Lett. **71**, 3641 (1993).

Sauer B.E., Wang Jun, and Hinds E.A., submitted to Phys. Rev. Lett. (1995).

Schiff L.I., Phys. Rev. **132**, 2194 (1963).

Smith J.H., Purcell E.M., and Ramsey N.F., Phys. Rev. **108**, 120 (1957).

Sushkov O.P, Flambaum V.V., and Khriplovich I.B. et al. JETP 60(5) 873 (1984)

Tonomura A, Matsuda T., Suzuki R., Fukuhara A., Osakabe N., Umezaki H., Endo J., Shinagawa K., Sugita Y., and Fujiwara H., Phys. Rev. Lett. **48**, 1443 (1982).

Wu C.S., Ambler E., Hayward R.W., Hoppes D.D., and Hudson R.P., Phys. Rev. **105**, 1413 (1957).

	Hot Wire?	A-X(nm)	$E_{int}(GV/cm)$
PbF	No	443	28
HgF	No	256*	96
YbF	OK	552	30
DyF	OK	?	?
BaF	Good	859	9

Table 4.1 Some properties of heavy paramagnetic fluorides. First column: detectability with hot wire. Second column: wavelength of first resonance line (* indicates C-X transition). Third column: effective electric field on the electron EDM.

Nature Lacks P Symmetry

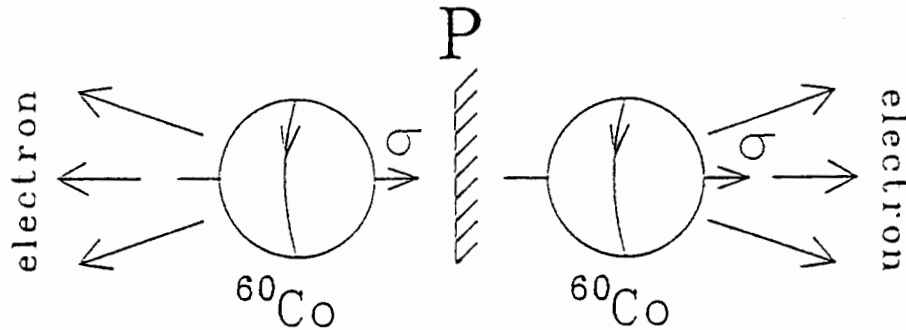


Fig. 1.1 Beta-decay of the ^{60}Co nucleus exhibits a corkscrew sense, thereby violating P symmetry.

The Happy Resolution

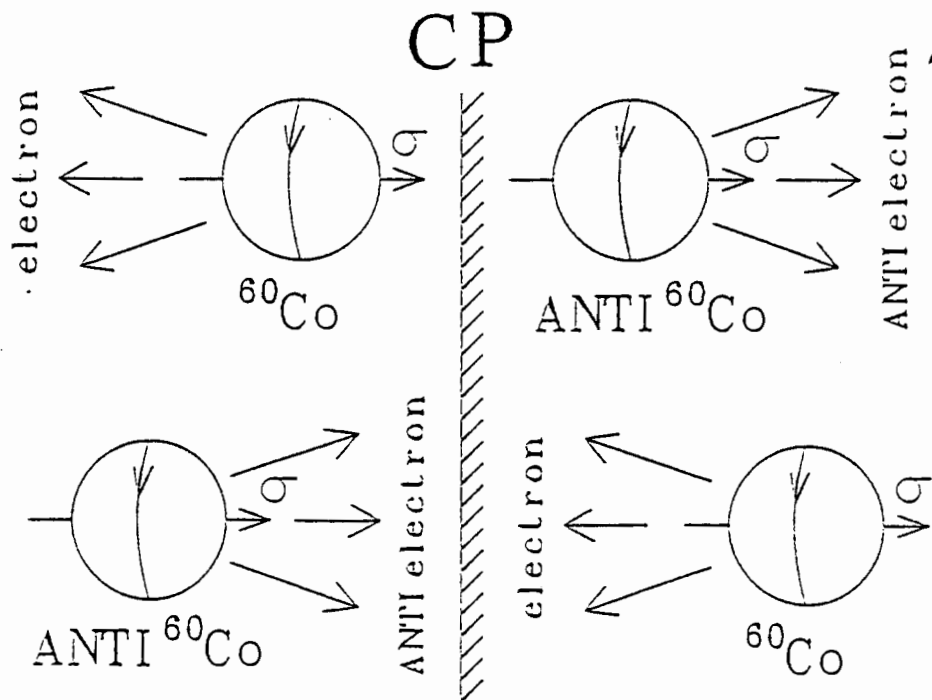
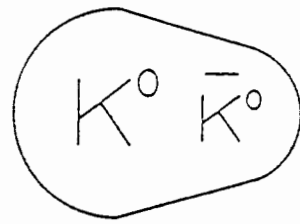


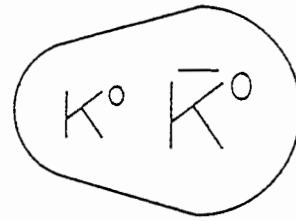
Fig. 1.2 If ^{60}Co and anti- ^{60}Co nuclei decay with opposite handedness, the world is the same after a CP transformation.

The CP-odd Kaon

CP



A kaon in its natural state



Not found in nature

Fig. 1.3 The long-lived kaon K_L^0 is a superposition of K^0 and \bar{K}^0 , with a slightly larger amplitude for K^0 . This violates CP symmetry.

P and T reflections of an Electric Dipole Moment

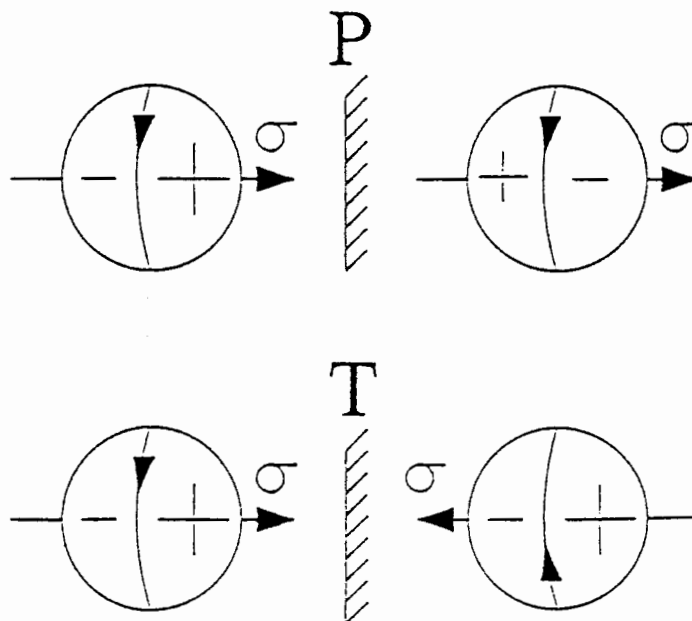


Fig. 1.4 An elementary system having angular momentum $\vec{\sigma}$ and a permanent electric dipole moment. This violates both P and T symmetry.

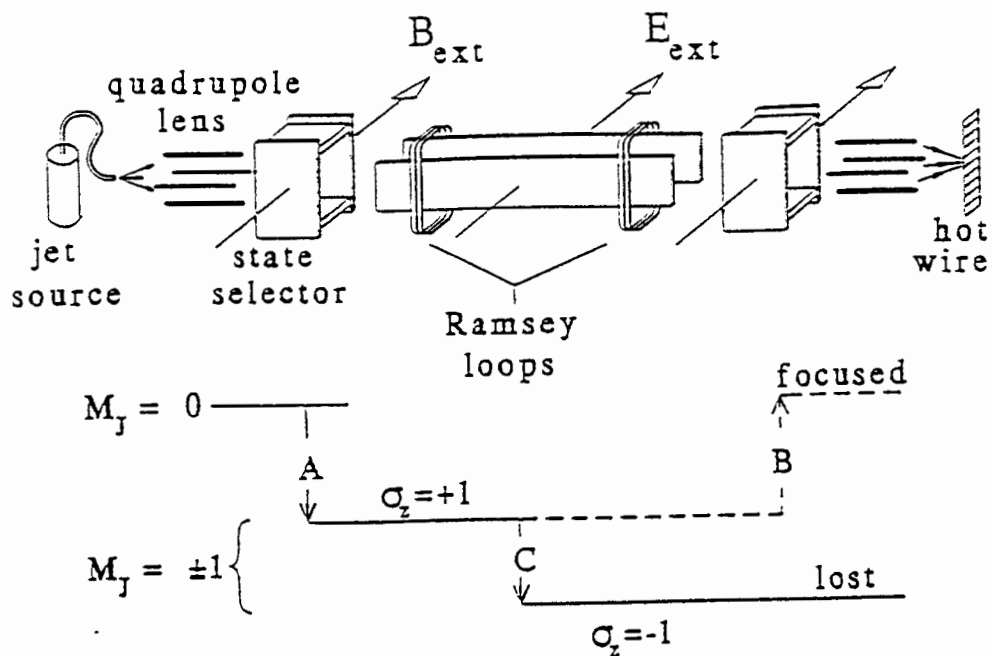


Fig. 2.1 Schematic diagram of TIF apparatus. State selector transition A places focused $M_J = 0$ molecules into a single magnetic sublevel of the $M_J = \pm 1$ manifold. Transition B is the inverse of A. The main resonance, labeled C, is the Tl nuclear spin flip.

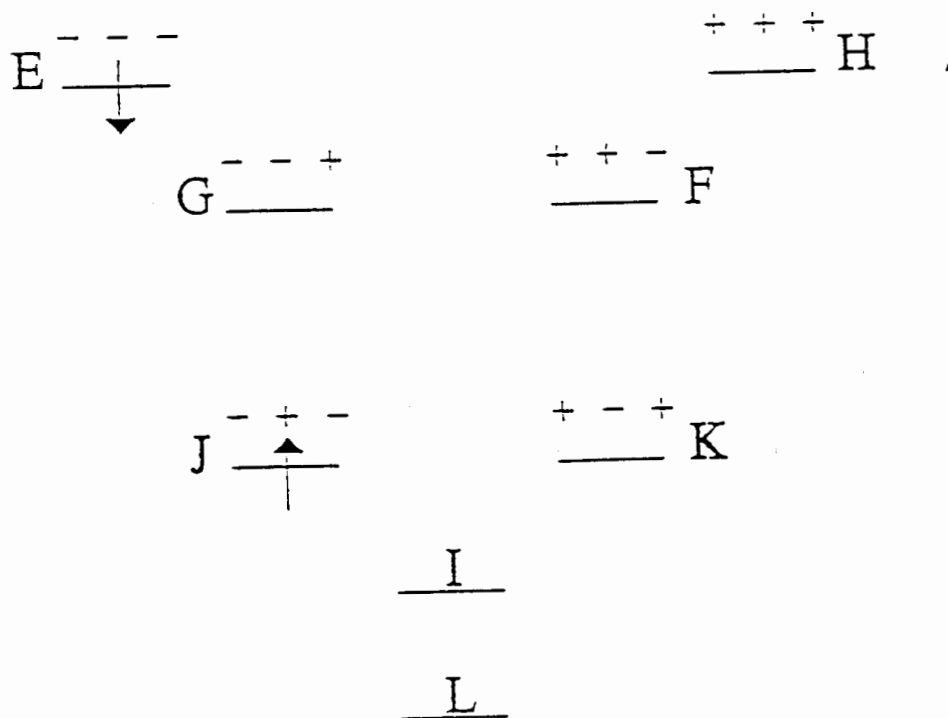


Fig. 2.2 The eight hyperfine sublevels having $M_J = \pm 1$ in high electric field. States are labeled by $M_J M_{Tl} M_F$ and by a letter. Thus state J has $M_J = -1, M_{Tl} = +1/2, M_F = -1/2$. States I and L are symmetric and antisymmetric superpositions of $(+ - -)$ and $(- + +)$. Arrows show the Tl spin flip relating states J and E.

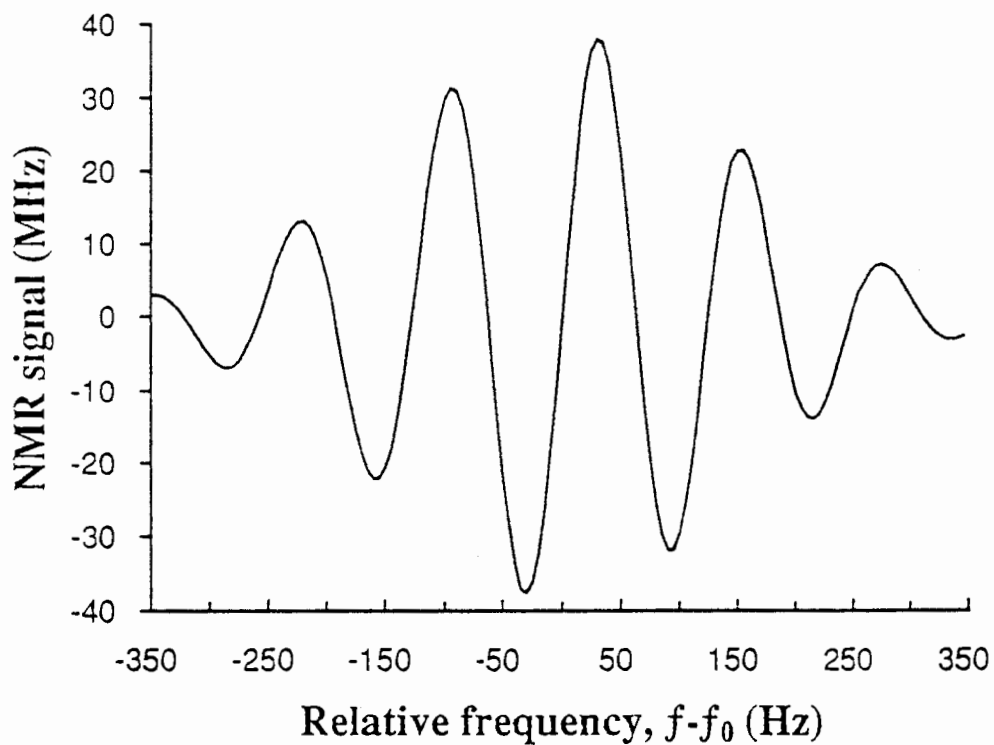
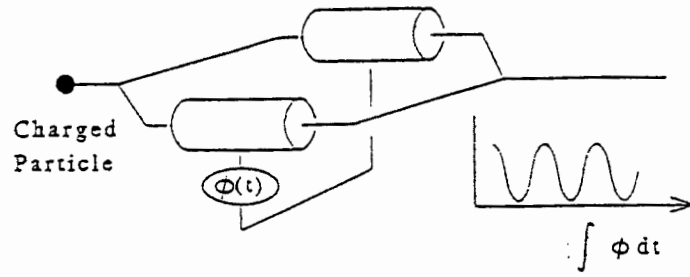


Fig. 2.3 Antisymmetric line shape of TI NMR signal produced by the separated oscillating field method. We plot the difference in the signal strength as the relative phase between the separated oscillating fields is switched between $+\pi/2$ and $-\pi/2$. The curve crosses zero at the resonance frequency $f_0 = 119.57$ kHz, and has a linewidth of 130 Hz. The slope of the line at resonance determined the sensitivity of the measurement.

Scalar Effect



Vector Effect

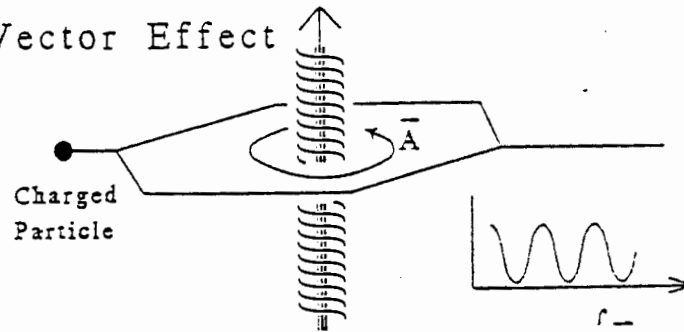
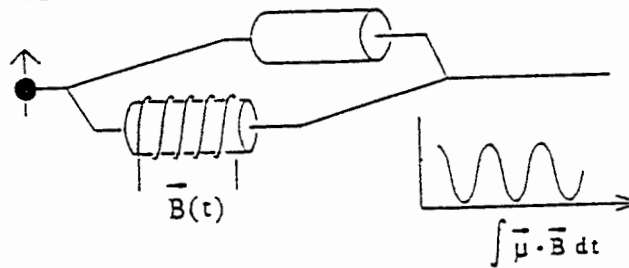


Fig. 3.1 Schemes for realizing the scalar and vector Aharonov-Bohm effects.

Scalar Effect



Vector Effect

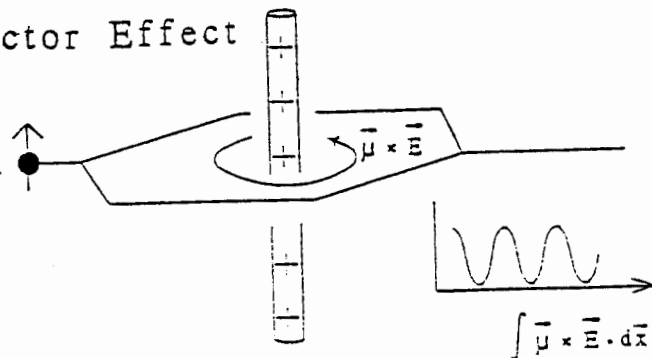


Fig. 3.2 Schemes for realizing the scalar and vector Aharonov-Casher effects.

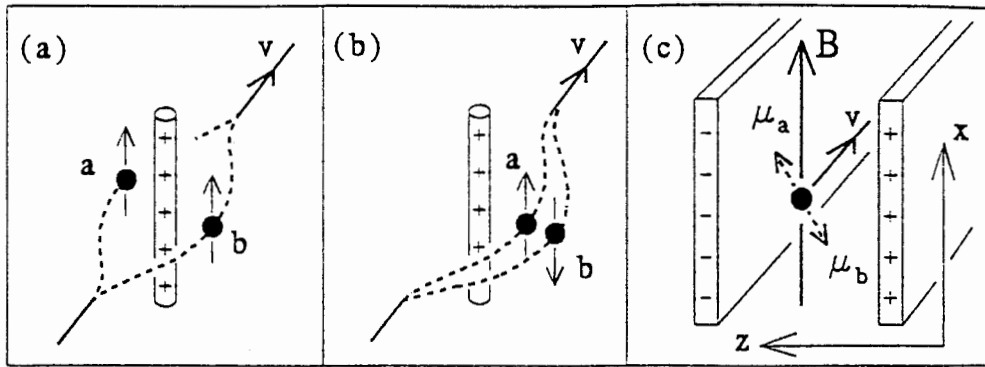


Fig. 3.3 Experimental configurations for observing the AC effect. (a) Geometry of the original measurement using a neutron interferometer, in which the two interfering states encircle a charge and have the same magnetic moments. (b) Alternative geometry in which the interfering states travel on the same path, but with different magnetic moments. (c) Geometry of the experiment by Sangster et al. (1993, 1995) using a uniform electric field, and a superposition of magnetic moments μ_a and μ_b . The polarizing magnetic field B_x is not shown here.

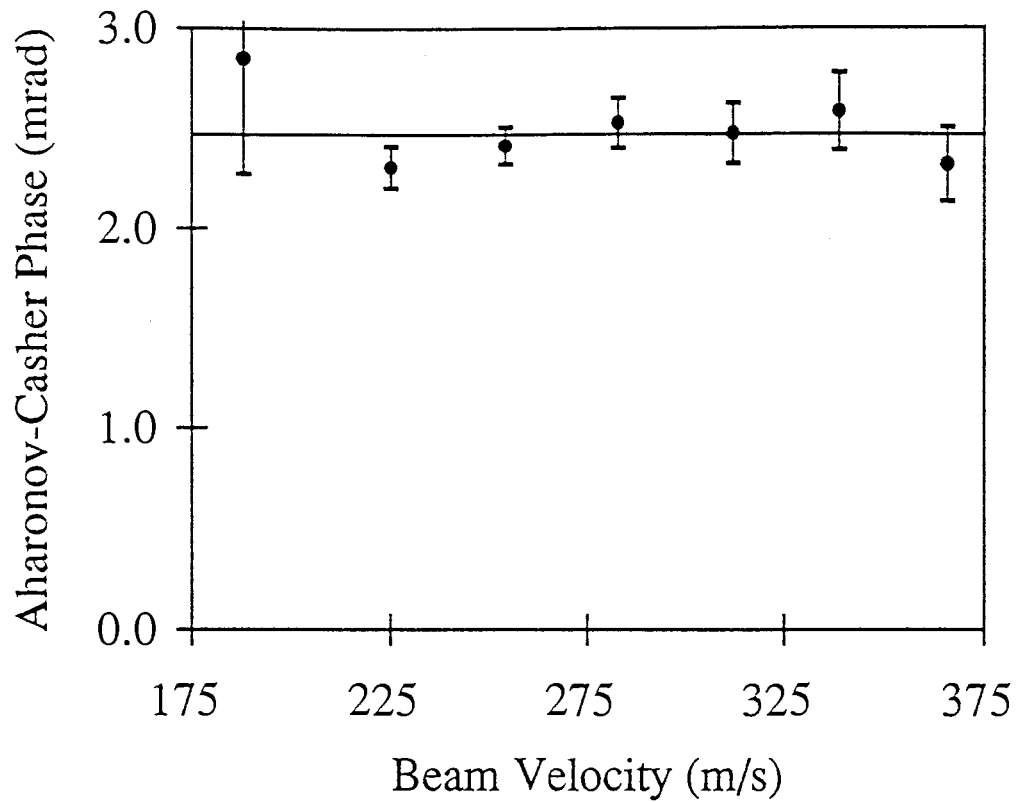


Fig. 3.4 AC phase versus beam velocity. The experimental points are in good agreement with the theoretical expectation. There are no free parameters.

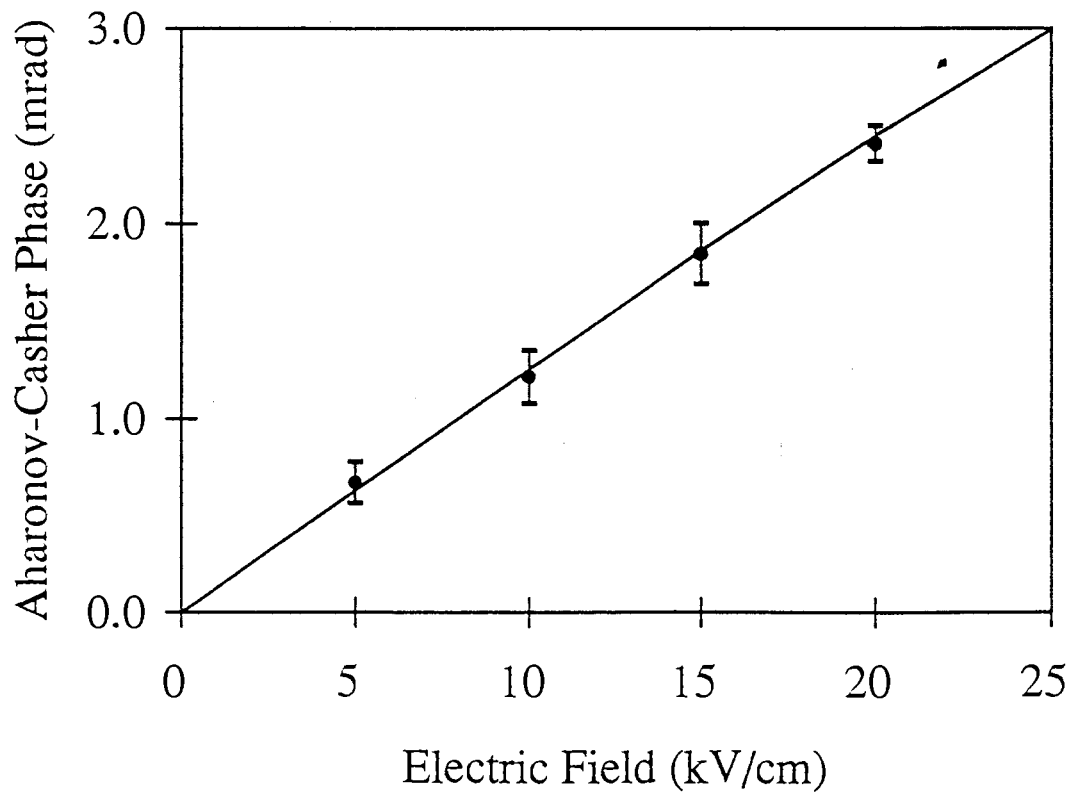


Fig. 3.5 AC phase versus electric field strength. The experimental points are in good agreement with the theoretical expectation. There are no free parameters.

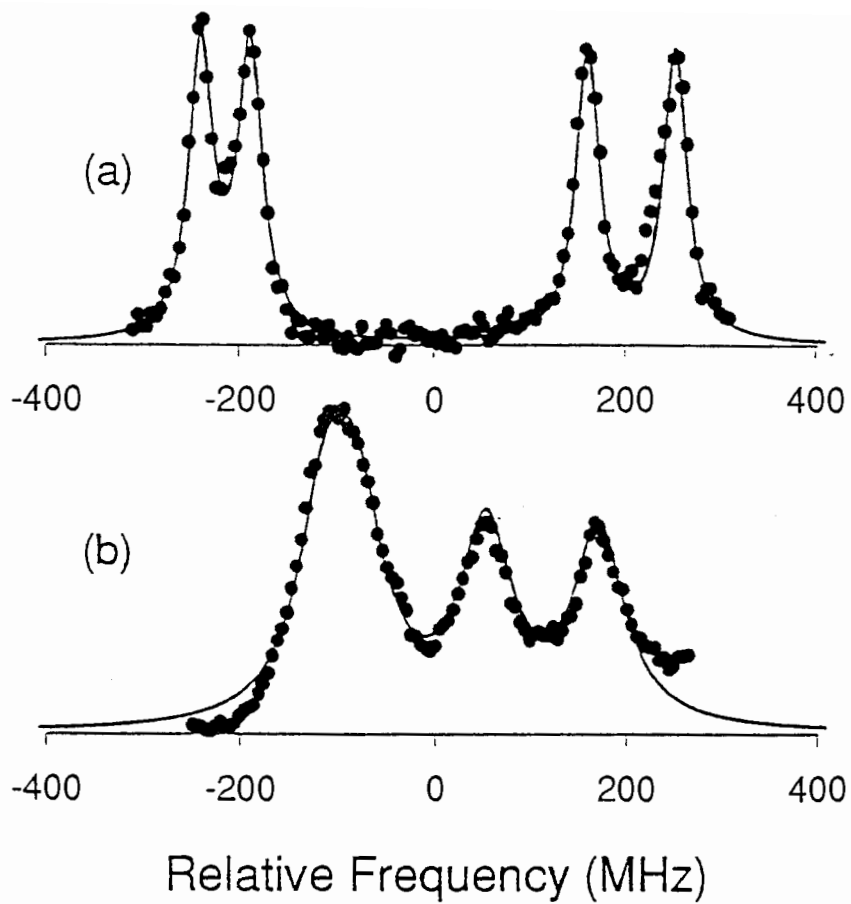


Fig. 4.1 Laser-induced fluorescence spectra of ^{174}YbF on the A-X transition. Upper trace: the P-branch lines for $N=70$. Lower trace: the P-branch lines for $N=13$. In each case, the points are experimental data and the line is the sum of four Lorentzians.

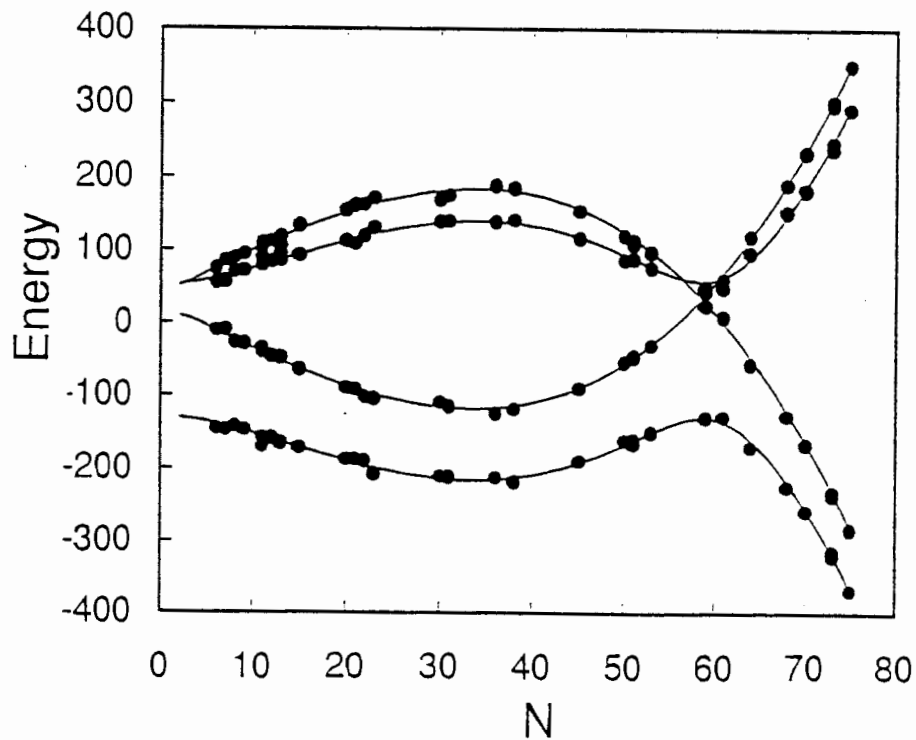


Fig. 4.2 Map of the four ground state levels of ^{174}YbF versus rotation N . Points are experimental. Lines are the best fit to the eigenvalues of Eq(4.14) with γ of the form $\gamma = \gamma_0 + \gamma_1 N(N + 1)$.

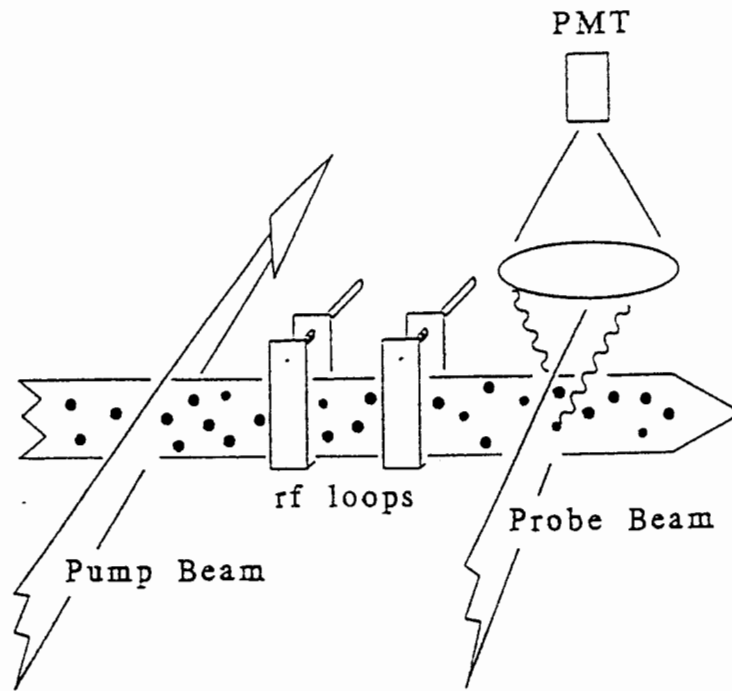


Fig. 4.3 General scheme for an experiment to measure the electron EDM using a YbF molecular beam.

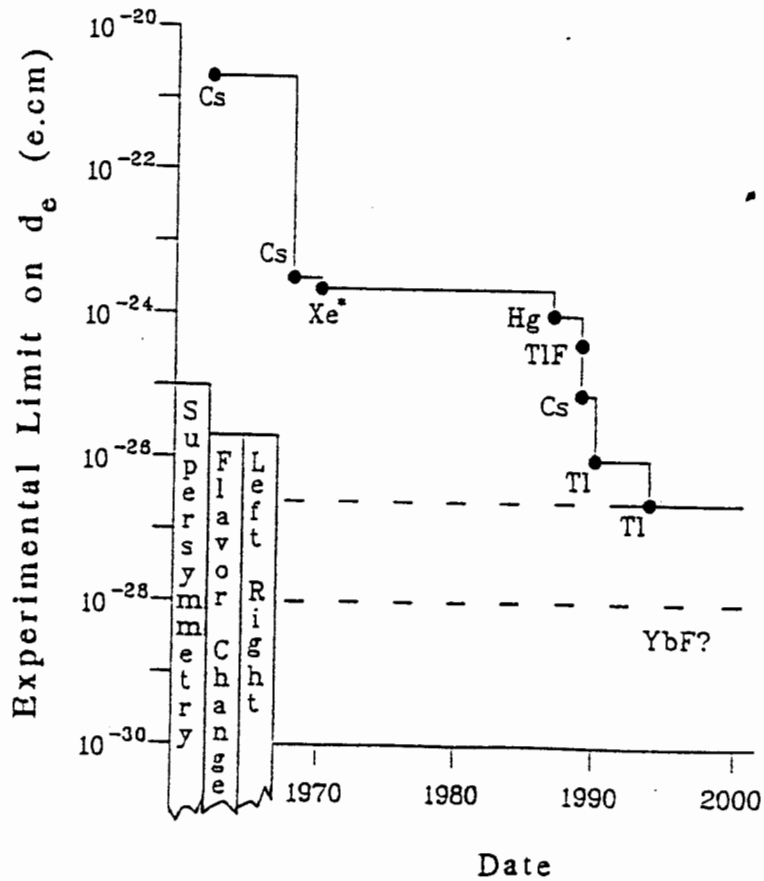


Fig. 4.4 A history of electron EDM measurements showing the experimental upper limit versus time. We also show possible values of d_e according to some extensions of the standard model.